

# The origin of the supersoft X-ray–optical/UV flux anticorrelation in the symbiotic binary AG Draconis

A. Skopal<sup>1</sup>, M. Sekeráš<sup>1</sup>, R. González-Riestra<sup>2</sup>, and R. F. Viotti<sup>3</sup>

<sup>1</sup> Astronomical Institute, Slovak Academy of Sciences, 059 60 Tatranská Lomnica, Slovakia

<sup>2</sup> XMM Science Operations Centre, ESAC, PO Box 78, 28691 Villanueva de la Cañada, Madrid, Spain

<sup>3</sup> INAF Istituto di Astrofisica Spaziale e Fisica Cosmica di Roma, via del Fosso del Cavaliere 100, 00133 Roma, Italy

Received / Accepted

## ABSTRACT

**Context.** AG Draconis produces a strong supersoft X-ray emission. The X-ray and optical/UV fluxes are in a strict anticorrelation throughout the active and quiescent phases.

**Aims.** To identify the source of the X-ray emission and reveal the nature of the observed flux anticorrelation.

**Methods.** The X-ray and UV observations with *XMM-Newton*, far-UV spectroscopy from *FUSE*, low- and high-resolution *IUE* spectra and optical/near-IR spectroscopic and/or photometric observations. Modeling the spectral energy distribution and broad wings of the O VI  $\lambda 1032$ ,  $\lambda 1038$  and He II  $\lambda 1640$  lines by the electron-scattering during the maximum of the 2003 burst, the following transition and quiescent phase.

**Results.** The X-ray–near-IR energy distribution at different levels of the star’s brightness confirmed quantitatively the observed flux anticorrelation and showed that the optical bursts are associated to an increase of the nebular component of radiation. The profile-fitting analysis revealed a significant increase in the mean particle density around the hot star from  $\sim 2.6 \times 10^{10} \text{ cm}^{-3}$  during quiescent phase to  $\sim 1.1 \times 10^{12} \text{ cm}^{-3}$  during the burst.

**Conclusions.** The supersoft X-ray emission is produced by the white dwarf photosphere. The X-ray and far-UV fluxes make it possible to determine its temperature unambiguously. The supersoft X-ray–optical/UV flux anticorrelation is caused by the variable wind from the hot star. The enhanced hot star wind gives rise to the optical bursts by reprocessing high-energy photons from the Lyman continuum to the optical/UV.

**Key words.** stars: binaries: symbiotic – stars: fundamental parameters – X-rays: binaries – X-rays: individuals: AG Dra

## 1. Introduction

Symbiotic stars are long-period (orbital periods are in order of years) interacting binaries consisting of a cool giant and a compact star, which is in most cases a white dwarf (WD), that accretes from the giant’s wind. This process generates a very hot ( $T_h \approx 10^5 \text{ K}$ ) and luminous ( $L_h \approx 10^2 - 10^4 L_\odot$ ) source of radiation, that ionizes a fraction of the neutral wind from the giant giving rise to *nebular* emission. As a result the spectrum of symbiotic stars consists of three basic components of radiation – two stellar and one nebular. (see e.g. Seaquist et al. 1984; Kenyon & Webbink 1984; Mürset et al. 1991; Skopal 2005). This situation represents the so-called *quiescent phase*, during which the symbiotic system releases its energy approximately at a constant rate and at a stable spectral energy distribution (SED). Sometimes, the symbiotic system changes its radiation significantly, brightens up by 1–3 magnitudes in the optical, shows signatures of a mass-outflow and changes its ionization structure for a few months to years (see e.g. Viotti et al. 1984; Corradi et al. 2003; Skopal 2005, and references therein). We name this stage as the *active phase*, and the corresponding brightening in the light curve is classified as the ‘Z And-type’ outburst. Occurrence of these outbursts is unpredictable and their nature is so far poorly understood (e.g. Sect. 1 in Sokolowski et al. 2006). Investigation of this type of outbursts represents the key problem in the research of symbiotic stars.

AG Dra is a yellow symbiotic binary comprising a K2 III giant (Mürset & Schmid 1999) and a WD accreting from the gi-

ant’s wind on a 549-day orbit (Fekel et al. 2000). The light curve of AG Dra shows numerous bursts with amplitude of 1–3 mag in *U* (Fig. 1). González-Riestra et al. (1999) identified *cool* and *hot* outbursts differing in their Zanstra temperatures and the light curve profile. The former are more pronounced ( $\Delta U \sim 3 \text{ mag}$ ) lasting for 1–2 years (e.g. 1981–83, 2006–07), while the latter are weaker ( $\Delta U \sim 1 - 2 \text{ mag}$ ), single brightenings lasting for weeks to months (e.g. 1985, 1986, 2003, see Fig. 1). Modeling the UV/IR continuum, Skopal (2005) found a significant contribution from the nebula in the near-UV/optical that strengthens during outbursts. The symbiotic nebula in AG Dra is dense. Material supplied by the giant’s wind into the binary environment at a rate of  $3 \times 10^{-7} M_\odot \text{ yr}^{-1}$  (Skopal 2005) corresponds to number densities of  $\approx 1 - 10 \times 10^8 \text{ cm}^{-3}$  in between the binary components and the neighbouring regions of similar dimensions. Therefore, to investigate properties of symbiotic nebula we can consider the Case *B* for its radiation (see Osterbrock 1989; Kwok 2000).

AG Dra is a halo binary system, placed at a galactic latitude of  $+41^\circ$  with a low reddening. Viotti et al. (1983) found  $E_{B-V} = 0.06 \pm 0.03$  by fitting the 2200 Å depression on the *IUE* spectra. Mikolajewska et al. (1995) re-analyzed a large number of *IUE* spectra and suggested  $E_{B-V} = 0.05 \pm 0.01$ , while Birriel et al. (2000) derived the extinction value of  $E_{B-V} = 0.08 \pm 0.01 \text{ mag}$  by fitting the UV spectra obtained by the Hopkins Ultraviolet Telescope. These quantities are comparable to the total reddening through the Galaxy towards AG Dra (0.07–

**Table 1.** Log of the used spectroscopic observations

Date YYYY/MM/DD	Julian date JD 24...	Stage*	Region [nm]	Observatory	$T_{\text{exp}}$ [s]
2003/10/06	52919.5	HB	330 - 1020	<i>Loiano</i>	660
2003/10/10	52923.7	HB	212	<i>XMM-OM</i>	1200
2003/10/10	52923.7	HB	1.93 - 6.92	<i>XMM-Newton</i>	17121 <sup>†</sup>
1985/03/13	46137.8	HB	115 - 335	<i>IUE</i>	600
1995/07/28	49927.5	HB	He II 164.0	<i>IUE</i>	5400
2003/11/14	52958.5	T	100 - 108.2	<i>FUSE</i>	4863
2003/11/19	52963.7	T	1.93 - 6.92	<i>XMM-Newton</i>	9217
2003/11/19	52963.7	T	212 - 291	<i>XMM-OM</i>	4400
2004/06/15	53172.0	Q	3.12 - 6.92	<i>XMM-Newton</i>	12354
2004/06/15	53172.0	Q	212 - 291	<i>XMM-OM</i>	4400
2004/06/24	53181.0	Q	100 - 108.2	<i>FUSE</i>	10832
1980/05/23	44383.1	Q	115 - 335	<i>IUE</i>	2520

\* hot burst (HB), transition to quiescence (T), quiescent phase (Q), <sup>†</sup> no detection of supersoft X-rays

0.08, Burstein & Heiles 1982), which justifies that the measured extinction to AG Dra is purely of the interstellar nature. From the Ly $\alpha$  width on high-resolution *IUE* spectra, Viotti et al. (1983) estimated the H I column density of  $\log N_{\text{H}} = 20.2$ . Using the Einstein X-ray observations, Aderson et al. (1981) found  $N_{\text{H}} = 3 \times 10^{20} \text{ cm}^{-2}$ . According to the relationship between  $N_{\text{H}}$  and  $E_{\text{B}-\text{V}}$  ( $N_{\text{H}}/E_{\text{B}-\text{V}} = 4.93 \times 10^{21} \text{ cm}^{-2} \text{ mag}^{-1}$ , Diplas & Savage 1994), both these parameters are consistent.

The orbital inclination of the binary is rather low. There are no signs of eclipses either in the optical, far-UV or X-ray regions (e.g. González-Riestra et al. 2008). Considering geometry of the main sources of radiation, Mikolajewska et al. (1995) estimated a system inclination  $i \approx 30^\circ - 45^\circ$  and Schmid & Schild (1997), based on spectropolarimetric observations, suggested  $i = 60 \pm 8^\circ$ . As a result we see the hot star rather from its pole than the orbital plane, where a disk-like structured material can be expected (e.g. Mastrodemos & Morris 1998). Both the low interstellar absorption/extinction and the low orbital inclination suggest a high transmission of the interstellar medium (ISM) to soft X-rays, which is consistent with the fact that AG Dra is the brightest system at these energies among other symbiotics. Therefore, AG Dra has been frequently observed by X-ray satellites.

Using the ROSAT observations Greiner et al. (1997) first noted a remarkable decrease of the X-ray flux during the optical (1994 and 1995) maxima, while in the UV and the optical they indicated a large increase of the emission line and continuum fluxes. They ascribed this X-ray/UV flux anticorrelation to a temperature decrease of the hot component. The X-ray history of AG Dra was recently reviewed and discussed by González-Riestra et al. (2008). They found that the anticorrelation between the X-ray and optical/UV emission appears to be a general feature of AG Dra radiation and is independent of the type and strength of the outburst. They suggested that during outbursts the WD radiation increases, but is strongly absorbed by the circumstellar ionized gas.

As the effect of the flux anticorrelation is related to transitions between active and quiescent phases, its understanding thus can aid us in revealing the nature of the Z And-type outbursts. Accordingly, in this paper we investigate the origin of the observed anticorrelation between the supersoft X-ray and the optical/UV fluxes for the case of AG Dra. For this purpose we model its composite continuum within the X-rays – near-IR domain at different levels of the activity. In Sect. 2 we summarize and describe nearly-simultaneous observations we used to model

the continuum. In Sect. 3 we describe our analysis and present the results. Their discussion and summary with conclusions are found in Sects. 4 and 5, respectively.

## 2. Observations

### 2.1. Sources of the data and their timing

For the aim of this paper we selected observations from the supersoft X-ray to the near-IR, taken at different levels of the AG Dra activity. We analyze the archival supersoft X-ray data made by the X-ray Multi-Mirror Telescope (*XMM-Newton*), including its Optical Monitor (*XMM-OM*) for the near-UV fluxes, the far-UV spectra (988 – 1082 Å) made with the LiF1A channel of the Far Ultraviolet Spectroscopic Explorer (*FUSE*), the ultraviolet low- and high-resolution spectra taken by the International Ultraviolet Explorer (*IUE*), the optical low-resolution spectrum from the Loiano observatory and the flux-points determined by the broad band optical *UBVR<sub>C</sub>I<sub>C</sub>* and near-IR *JHKLM* photometry. The *XMM-Newton* and Loiano observations were described in detail by González-Riestra et al. (2008). The *FUSE* spectra were processed according to Skopal et al. (2006).

During quiescent phase we composed the observed SED by the *XMM-Newton* and *FUSE* observations, complemented with the *IUE* spectrum (SWP9084/LWR07831) taken at a similar orbital position. During transition phase we selected the near-simultaneous *XMM-Newton* and *FUSE* observations and the photometric *UBV* flux-points from the descending branch of the 2003 burst (Fig. 1). To model the SED at the maximum of hot bursts we used the ultraviolet *XMM-OM* fluxes and the optical spectrum, both from the maximum of the 2003 burst. However, to estimate the relevant far-UV fluxes we had to use a non-simultaneous observation. We used well-exposed *IUE* spectra (SWP25443/LWP05513) taken around the maximum of the 1985 hot burst. To match the *XMM-OM* fluxes we scaled the *IUE* spectrum by a factor of 1.3. This was possible, because hot bursts are similar in their profiles and colours (see Fig. 1 here and Fig. 6 of González-Riestra et al. 1999, for UV colours). Their SED shows a dominant contribution from the nebula to the near-UV/U region, while the hot stellar source dominates the far-UV region (see Fig. 13 of Skopal 2005).

For the profile-fitting analysis we used the O VI  $\lambda 1032, \lambda 1038$  doublet on the *FUSE* spectra, available from the quiescent and transition phases. For the optical maximum we analyzed the He II  $\lambda 1640$  line exposed on the high-resolution *IUE* spectra

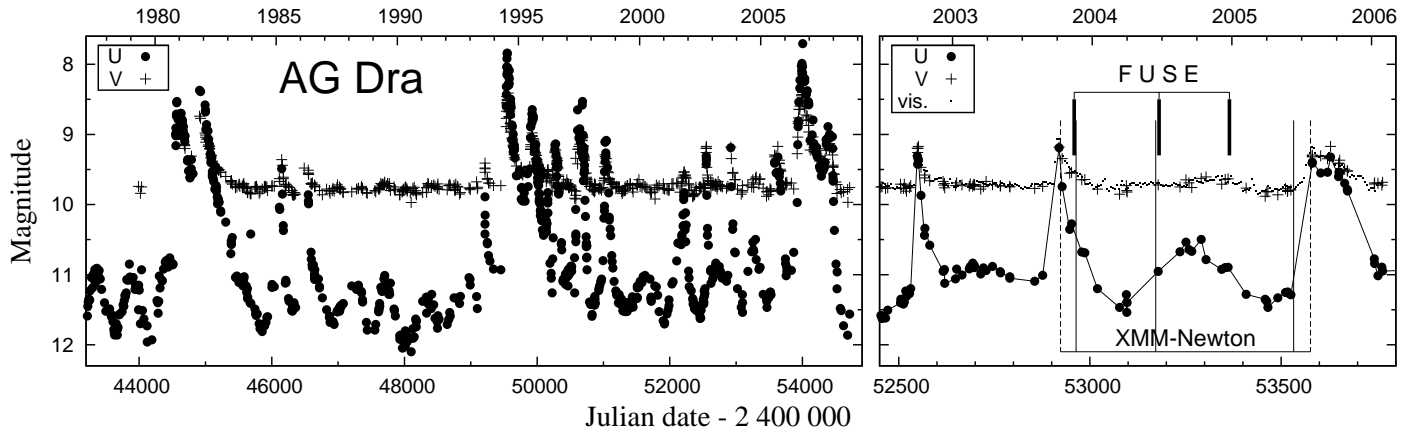


**Fig. 1.** The *U* and *V* light curves of AG Dra from 1977. They are characterized with a series of outbursts with multiple maxima. The data were summarized by Skopal et al. (2007). The right panel shows a detail around the 2003 hot burst with timing of the *XMM-Newton* (long thin lines) and the *FUSE* (short thick bars) observations. During the optical maxima, the soft X-ray emission was not detectable (long dashed lines).

(SWP55372 and SWP55373) at the maximum of the 1995 hot burst. The spectra were calibrated with the aid of their low-resolution counterparts.

Relevant observations were dereddened with  $E_{B-V} = 0.08$  and resulting parameters were scaled to a distance of 1.1 kpc (Birriel et al. 2000; Skopal 2005). Their log and plots are given in Table 1 and Fig. 2, respectively.

## 2.2. Derivation of the X-ray fluxes

In this paper we analyze observations of AG Dra made by *XMM-Newton* (Jansen et al. 2001), performed during the 2003 hot burst (at its optical maximum and transition to quiescence) and during quiescent phase (Fig. 1). Details of the observations and the data reduction were already described by González-Riestra et al. (2008). To estimate the X-ray fluxes we fitted the spectra from the EPIC-pn instrument with the XSPEC software package. According to a very high temperature of the hot stellar source in AG Dra ( $> 10^5$  K, Kenyon & Webbink 1984; Mürset et al. 1991; Greiner et al. 1997; Skopal 2005) we can assume that the supersoft X-ray fluxes are emitted by the WD photosphere. Therefore, we considered a simple temperature blackbody model in fitting our 0.18–0.4 keV data. The resulting fit to the spectrum from quiescence corresponded to the blackbody radiation absorbed with the hydrogen column density  $N_{\text{H}} \sim 3 \times 10^{20} \text{ cm}^{-2}$  and temperature of  $\sim 14.5$  eV as in the case of the ROSAT PSPC observations from quiescence (see Greiner et al. 1997; González-Riestra et al. 2008). During the transition, the shape of the spectrum was similar, but the lower signal to noise ratio prevented a meaningful fit. In this case we assumed the same parameters as for the quiescence spectrum, and thus fitted only the normalization factor. Fluxes were derived from these ‘unfolded’ models and the corresponding data/model ratio. This approach implies that the fluxes obtained by this way are, to a certain extent, model dependent. However, we are confident that the spectrum can be well represented by a simple absorbed blackbody model, which is also supported by the data-minus-model residuals that are small, flat and within the errors in the range of 40–70 Å. Here we refer the reader to the paper of Nowak et al. (2002), who discuss other approaches to obtaining flux points from X-ray data and the effects connected with. To

assess influence of the hydrogen column density and the temperature in the derived fluxes we fitted the data with a few hundred of models covering a wide range of these parameters. Taking the 30 best fit cases (in terms of  $\chi^2$ ), we found that the fluxes derived from these models differ from the resulting ones by less than 15% in the range of 30–65 Å. Uncertainties of the X-ray fluxes derived in this way satisfy the purposes of this work. Further, we complemented the X-ray fluxes with those from the *FUSE* spectra to determine final parameters of the radiation produced by the WD photosphere (see below, Sect. 3.1.1.).

## 3. Analysis and results

### 3.1. Modeling the composite spectrum

The continuum spectrum of symbiotic stars is composed of three basic components of radiation – two stellar,  $F_{\text{h}}(\lambda)$  and  $F_{\text{g}}(\lambda)$ , from the hot star and the cool giant, respectively, and one nebular,  $F_{\text{n}}(\lambda)$ , from the ionized gas in the system (Sect. 1). Their superposition then yields the observed flux as

$$F(\lambda) = F_{\text{g}}(\lambda) + F_{\text{h}}(\lambda) + F_{\text{n}}(\lambda). \quad (1)$$

To achieve our aim we need to determine physical parameters of the hot stellar and the nebular component of radiation during different stages of the activity. We will use the method of disentangling the composite spectrum of S-type symbiotic stars as proposed by Skopal (2005). Observations from the soft X-rays to the near-IR cover well all the energy domains, within which the individual components of radiation have a dominant contribution. This allows us to model them separately. In the following three sections we describe our approximations of these components of radiation.

#### 3.1.1. The hot star continuum

According to Greiner et al. (1997) and Viotti et al. (2005) the soft X-ray radiation in AG Dra could be associated with the hot star photosphere. However, the soft X-rays from cosmic sources are significantly attenuated by absorptions in the ISM, which requires relevant correction before their interpretation (e.g. Cruddace et al. 1974; Wilms, Allen & McCray 2000).

Assuming that no emission occurs on the path between the X-ray source and the observer, we can use the simplest solution of the radiative transfer equation to correct the observed X-ray flux,  $F_x^{\text{obs}}(\lambda)$ , for absorptions as

$$F_x^{\text{obs}}(\lambda) = F_x(\lambda) e^{-\tau_\lambda}, \quad (2)$$

where  $F_x(\lambda)$  is the X-ray spectrum as emitted by the source and  $\tau_\lambda$  is the optical depth along the line of sight. It is given by the absorption cross-section per atom,  $\sigma_i(\lambda)$ , of the element,  $i$ , and the total number of atoms on the line of sight,  $\sum_i n_i$ . Thus,  $\tau_\lambda = \sum_i n_i \sigma_i(\lambda) = \sum_i a_i \sigma_i(\lambda) N_H = \sigma_X(\lambda) N_H$ , where  $a_i$  is the relative abundance,  $N_H$  is the total hydrogen column density [ $\text{cm}^{-2}$ ] and  $\sigma_X(\lambda)$  [ $\text{cm}^2$ ] is the total cross-section of the material on the line of sight per hydrogen atom in the X-ray domain (e.g. Cruddace et al. 1974).

In addition to the X-ray fluxes from *XMM-Newton*, we use the far-UV continuum fluxes between  $\lambda 1188$  and  $\lambda 1000 \text{ \AA}$ , made nearly-simultaneously with the *FUSE* satellite (see Fig. 1). As we analyze both the X-ray and the far-UV data, we consider attenuation of the light by bound-free absorptions in the X-ray domain and by the interstellar extinction in the far-UV spectrum. According to previous models (see Sect. 2.2.), we approximate the hot stellar continuum by a blackbody radiation at a temperature  $T_h$ . As a result, and in the sense of Eq. (2), we model the hot star continuum by fitting the observed X-ray/far-UV fluxes,  $F_h^{\text{obs}}(\lambda)$ , with a function

$$F_h^{\text{obs}}(\lambda) = \begin{cases} \theta_h^2 \pi B_\lambda(T_h) e^{-\sigma_X(\lambda) N_H} & \text{for } \lambda < 912 \text{ \AA} \\ \theta_h^2 \pi B_\lambda(T_h) 10^{-0.4 R k_\lambda E_{B-V}} & \text{for } \lambda > 912 \text{ \AA} \end{cases} \quad (3)$$

where the scaling factor  $\theta_h = R_h^{\text{eff}}/d$  is given by its effective radius  $R_h^{\text{eff}}$  and the distance  $d$ , and thus represents the angular radius of the hot stellar source. The observed far-UV fluxes were corrected using the extinction curve  $k_\lambda$  of Cardelli et al. (1989) and the ratio of total to selective extinction  $R = 3.1$  (e.g. Wegner 2003). In addition to the attenuation effects included in Eq. (3), the neutral hydrogen on the line of sight causes a depression of the continuum around hydrogen lines of the Lyman series due to the Rayleigh scattering (Isliker et al. 1989). By analogy to the first term of Eq. (3) we can express the Rayleigh attenuated continuum as

$$F_h^{\text{obs}}(\lambda) = \theta_h^2 \pi B_\lambda(T_h) e^{-\sigma_R(\lambda) N_H}, \quad (4)$$

where  $\sigma_R(\lambda)$  is the Rayleigh scattering cross-section for atomic hydrogen. On our *FUSE* spectra the effect is seen around the Ly- $\beta$  line (Fig. 2), and can be used to test quantity of  $N_H$  obtained from the X-ray domain.

### 3.1.2. The nebular continuum

We approximate the nebular component of radiation in the UV/optical continuum by processes of recombination and thermal bremsstrahlung in the hydrogen plasma, radiating under conditions of the Case *B*. Validity of this simplification is supported by the following arguments: (i) A strong nebular continuum is characterized with a simple and low electron temperature of  $T_e \sim 2 \times 10^4 \text{ K}$  (Table 3), which suggests that the nebula is powered mainly by photoionization, i.e. ionizations by collisions are not important. (ii) There are no recognizable signatures of the He II continuum in the *IUE* spectra (e.g. a jump in emission at  $\sim 2050 \text{ \AA}$  and/or a pronounced Paschen series of the He II

recombination lines). Also it is not possible to separate contributions from the He I continuum, because of its very similar recombination coefficients to that of H I (e.g. Brown & Mathews 1970) and a small abundance. That is why we consider nebular emission from hydrogen only. (iii) Symbiotic nebulae are relatively very dense (Sect. 1). This makes the mean-free path of any diffuse Lyman continuum photons to be too short to escape the nebula, i.e. the nebula is optically thick in the Lyman continuum. This means that the ionizations caused by stellar radiation-field photons are balanced by recombinations to excited levels of H I, while the ground state in the recombination process can be ignored. Therefore we consider the Case *B* for the nebular radiation. (iv) Because of the high density, we can neglect contributions due to the two-photon emission.

According to these simplifications and with the aid of Eq. (11) in Skopal (2005), the  $F_n(\lambda)$  term in Eq. (1) here can be expressed as

$$F_n(\lambda) = \frac{EM}{4\pi d^2} \varepsilon_\lambda(H, T_e), \quad (5)$$

where  $\varepsilon_\lambda(H, T_e)$  [ $\text{erg cm}^3 \text{ s}^{-1} \text{ \AA}^{-1}$ ] is the volume emission coefficient for hydrogen, which depends on the electron temperature  $T_e$  and is a function of wavelength (e.g. Brown & Mathews 1970). We note that the observed nebular emission represents only the optically thin part of the symbiotic nebula (Skopal 2001). This implies that the measured  $EM$  represents a lower limit of that originally created by ionizations, which puts a lower limit to the required flux of ionizing photons (see Eq. (6) below).

### 3.1.3. Radiation from the giant

For the stellar radiation from the giant in AG Dra we adopt the model SED according to Skopal (2005). The model is based on the optical *VRI* and the near-IR *JHKLM* flux points matched by a synthetic spectrum calculated for the effective temperature of 4300 K. This spectrum then defines the first term in Eq. (1),  $F_g(\lambda)$ . Its bolometric flux,  $\theta_g^2 \sigma T_{\text{eff}}^4 = 9.51 \times 10^{-9} \text{ erg cm}^{-2} \text{ s}^{-1}$ , corresponds to the giant's radius  $R_g = 33 (d/1.1 \text{ kpc}) R_\odot$  and the luminosity  $L_g = 360 (d/1.1 \text{ kpc})^2 L_\odot$ .

### 3.2. Thomson-scattering wings of O VI $\lambda 1032$ , $\lambda 1038$ and He II $\lambda 1640$ lines

The aim of this section is to model the extended wings of the O VI and He II lines measured at similar levels of the optical brightness, at which the X-ray observations were carried out. By this way we support the results obtained by model SEDs.

Schmid et al. (1999) suggested that the broad wings of the O VI  $\lambda 1032$  and  $\lambda 1038$  resonance lines could be explained by scattering of the O VI photons by free electrons. The effect of this process is weak and wavelength independent, because of a very small and constant value of the Thomson cross-section,  $\sigma_T = 6.652 \times 10^{-25} \text{ cm}^2$ . However, the densest portions of the symbiotic nebula ( $\log(n_e) \sim 8 - 12 \text{ cm}^{-3}$ ) extending to a few AU could be sufficiently optically thick for the electron-scattering process. Qualitatively, the effect should be more significant during active phases, because of a surplus of electrons from the increased hot star wind (e.g. Skopal 2006). Especially, the strong emission lines of highly ionized elements that are formed in the densest part of the hot stellar wind represent the best candidates for a well measurable effect of the Thomson scattering.

To calculate the electron-scattering wing profiles we adopted the procedure suggested by M $\ddot{u}$ nch (1950) that assumes the

**Table 2.** Parameters of the profile-fitting analysis (Sect. 3.2, Fig. 2)

Date	Stage	Line	$\tau_e$	$T_e$ [K]	$\chi^2_{\text{red}}$	$\bar{n}_e$ [cm <sup>-3</sup> ]
1995/07/28	HB	He II	0.32	28 800	0.9	$1.1 \times 10^{12}$
2003/11/14	T	O VI	0.083	28 500	1.2	$1.7 \times 10^{11}$
2004/06/24	Q	O VI	0.061	20 300	0.8	$2.6 \times 10^{10}$

electron scattering happens in the layer outside the line formation region, and that the electrons are segregated from the other opacity sources, which implies no change in the equivalent width of the line. Further we used the expression of Castor et al. (1970) for the resulting scattered line profile and the electron-scattering redistribution function derived by Hummer & Mihalas (1967). This simplified approach was used by many authors, recently by Young et al. (2005).

In our profile-fitting analysis, we approximated the observed P Cygni-type of the O VI line profiles by two Gaussians and fitted their broad wings with 2 free parameters – the electron temperature,  $T_e$ , and the electron-scattering optical depth,  $\tau_e$ . Removing emission/absorption features and bumps in the profiles we fitted the broad wings in the range of about  $\pm 10 \text{ \AA}$  around the line cores using 644, 1004 and 370 flux-points in the wing profile from quiescence, transition and burst stage, respectively. The resulting fits for all three cases we analyzed have small reduced  $\chi^2_{\text{red}} \lesssim 1$  (Table 2, Fig. 2), which implies that mean residuals are comparable to the errors of the modeled flux-points. Thus the model fits well the broad wings of the profile, which confirms their origin as due to the electron-scattering. A detailed description of our approach will be presented elsewhere (Sekeráš & Skopal 2009).

A comparison of our model SEDs and profiles with observations is plotted in Fig. 2 and corresponding parameters are given in Tables 2 and 3.

### 3.3. The SED-fitting analysis

#### 3.3.1. Parameters of the hot stellar source

To derive parameters of the hot stellar source in AG Dra, the following points are relevant.

(i) We dereddened the *FUSE* fluxes and calculated the Rayleigh scattering effect around Ly- $\beta$  (Eq. (4)) to estimate  $N_H$ . The scattering cross-section,  $\sigma_R(\lambda)$ , was calculated according to Nussbaumer et al. (1989). However, numerous and strong absorptions in the *FUSE* spectrum did not allow us to determine unambiguously the  $N_H$  parameter. Therefore, we could only compare the Rayleigh attenuated blackbody radiation to the observed continuum for a reasonable range of  $N_H$  quantities. We found that the observed depression in the continuum around Ly- $\beta$  constrains  $N_H$  to  $\sim 2 - 4 \times 10^{20} \text{ cm}^{-2}$  that is consistent with the values suggested by different methods (Sect. 1).

(ii) We calculated a grid of synthetic models of the function (3) for reasonable ranges of the fitting parameters,  $\theta_h$ ,  $T_h$  and  $N_H$ . We compared models to both the observed X-ray and dereddened UV fluxes, and used the  $\chi^2$  statistics to evaluate the fit. To correct the observed X-ray fluxes for absorptions we used the *tbabs* absorption model (Tübingen-Boulder absorption ISM model, Wilms, Allen & McCray 2000). During the quiescent phase we fitted 11 X-ray fluxes from 31 to 69  $\text{\AA}$  and three far-UV flux-points around 1000  $\text{\AA}$  (bottom left panel of Fig. 2).

We estimated errors in the X-ray fluxes to be of 2–17% of their mid values, while for the *FUSE* spectra we adopted errors as large as 5–10% of the measured continuum. The best-fit-model and the flux-point errors yielded  $\chi^2 = 34.6$  and  $\chi^2_{\text{red}} = 3.1$  for 11 degrees of freedom (dof). As the model fits well the data, the somewhat larger  $\chi^2_{\text{red}}$  reflects rather small values of our error estimates. During the transition stage we fitted 7 X-ray fluxes between 43 and 69  $\text{\AA}$  and three far-UV flux-points. We omitted fluxes around 20–30  $\text{\AA}$ , because of their different nature. They could be originated by shocks in the nebula. Flux uncertainties we used, were estimated to be in the range of 7–22%. The resulting fit has a small  $\chi^2_{\text{red}} = 0.6$  for 7 dof, which suggests that the model fits the data very closely, well within their uncertainties. Corresponding best-fit-model parameters and their derivatives (the effective radius and the luminosity of the hot stellar source) are introduced in Table 3.

(iii) During the bursts, when the supersoft X-ray emission is absorbed entirely, it is not possible to determine unambiguously the hot star temperature for  $T_h \gtrsim 10^5 \text{ K}$ , because of too small range of the far-UV fluxes available. Nevertheless, we can estimate a lower limit of the temperature of the ionizing source,  $T_h^{\text{min}}$ , at which the hot star radiation, scaled to the far-UV fluxes, is just capable of producing the observed *EM*, i.e. the total number of ionizing photons just balances the total number of recombinations. According to simplifications for the plasma radiation as introduced in Sect. 3.1.2., we solve equilibrium equation (Eq. 6 below) for the temperature  $T_h$  and the scaling factor  $\theta_h^2$ , which determine the flux of ionizing photons, with the input parameters of the measured nebula, *EM* and  $T_e$ . The resulting temperature then corresponds to  $T_h^{\text{min}}$ , at which the hot star radiation gives rise to the observed nebular emission (see Skopal 2005, in detail).

#### 3.3.2. Parameters of the nebula

According to Eq. (1), the nebular component of radiation can be obtained by subtracting the stellar contributions from the observed spectrum, i.e.  $F_n(\lambda) = F(\lambda) - F_h(\lambda) - F_g(\lambda)$ . First, we estimated representative continuum fluxes at about 20 wavelengths between 1250 and 3300  $\text{\AA}$  and complemented them with photometric *U* and *XMM-OM* fluxes, if available. Uncertainties of the well exposed spectra from the *IUE* archive are between 5 and 10% of the measured values. Errors in the *XMM-OM* fluxes were estimated to only a few percents (see Table 2 in González-Riestra et al. 2008). Uncertainties of classical photometric measurements can be assumed to be less than 10%. We corrected corresponding fluxes for the influence of emission lines using our Loiano spectra (see Skopal 2007, in detail). Second, we subtracted the contribution of the WD and the giant and fitted the function  $F_n(\lambda)$  given by Eq. (5) to the corrected flux-points to determine the *EM* and  $T_e$  of the symbiotic nebula. Resulting fits have  $\chi^2_{\text{red}} \lesssim 1$  that proves assumptions of our simplified model of the nebula (Sect 3.1.2.). Corresponding plots and parameters are in Fig. 2 and Table 3, respectively.

## 4. Discussion

### 4.1. Model SEDs and the flux anticorrelation

Model SEDs show that the light variations in the optical/near-UV, as measured at different levels of activity, are caused exclusively by the variable nebular continuum (Fig. 2, Table 3). Contribution from the hot stellar object can be neglected within this domain, and that from the giant can be assumed to be constant.

**Table 3.** Parameters of the SED-fitting analysis (see Sect. 3.3, Fig. 2).

Stage	$N_{\text{H}}$ [cm <sup>-2</sup> ]	$T_{\text{h}}$ [K]	$\theta_{\text{h}}$	$R_{\text{h}}^{\text{eff}}$ [ $R_{\odot}$ ]	$L_{\text{h}}$ [ $L_{\odot}$ ]	$L_{\text{ph}}(\text{H})$ [s <sup>-1</sup> ]	$\chi_{\text{red}}^2$	$T_{\text{e}}$ [K]	$EM$ [cm <sup>-3</sup> ]	$\chi_{\text{red}}^2$
HB	$>2.5 \times 10^{21}$	$>180\,000$	$<8.9 \times 10^{-13}$	$<0.043$	$>1\,760$	$>8.9 \times 10^{46}$	–	18 600	$6.2 \times 10^{59}$	1.3
T	$3.27 \times 10^{20}$	146 200	$7.3 \times 10^{-13}$	0.036	530	$3.1 \times 10^{46}$	0.6	21 500	$2.2 \times 10^{59}$	0.8
Q	$2.82 \times 10^{20}$	164 400	$6.3 \times 10^{-13}$	0.031	630	$3.4 \times 10^{46}$	3.1	21 000	$1.3 \times 10^{59}$	0.4

The nebular component of radiation represents a fraction of the hot stellar radiation transformed by the ionization/recombination events throughout the symbiotic nebula. The result of this process depends on the number of ionizing photons ( $L_{\text{ph}}$  [s<sup>-1</sup>]) produced by the hot star and the number of particles on their path that are subject to ionization. In the case of the hydrogen plasma (see Sect. 3.1.2.) characterized with one  $T_{\text{e}}$  and a mean particle concentration,  $\bar{n}$ , the equilibrium condition between  $L_{\text{ph}}$  photons and the number of recombinations can be expressed as

$$L_{\text{ph}}(\text{H}) = \int_V n_{\text{e}} n^+ \alpha_{\text{B}}(\text{H}, T_{\text{e}}) dV = \alpha_{\text{B}}(\text{H}, T_{\text{e}}) \bar{n}^2 V \quad (6)$$

$$= \alpha_{\text{B}}(\text{H}, T_{\text{e}}) EM,$$

where  $\alpha_{\text{B}}(\text{H}, T_{\text{e}})$  [cm<sup>+3</sup> s<sup>-1</sup>] is the recombination coefficient to all but the ground state of hydrogen (i.e. the Case B). For parameters of AG Dra during quiescence, the equilibrium condition is satisfied at the locus of points in directions from the hot to/around the cool star, where the flux of  $L_{\text{ph}}$  photons are balanced by the flux of the neutral atoms of hydrogen in the wind from the giant. Throughout the remainder part of the nebula  $L_{\text{ph}} > \alpha_{\text{B}} EM$ , which means that a fraction of  $L_{\text{ph}}$  photons escapes the nebula without being transformed to the nebular radiation (see Appendix B and Fig. 3 in Skopal 2001). Under these conditions, new particles injected into such the nebula will consume the surplus of ionizing photons, what consequently will increase the nebular emission observed during the bursts. This situation can naturally be explained by a strengthened wind from the WD, that also induces an increase of the optical depth in the continuum in the direction of the WD, what we indicate by its larger effective radius in comparison with values from quiescence (Table 3).

According to Eq. (2) and the relatively large values of  $\sigma_{\text{X}}$  in the supersoft X-ray domain, a small increase of  $N_{\text{H}}$  in between the source and the observer produces a significant attenuation of the  $F_{\text{x}}(\lambda)$  fluxes. For example, comparison of our *XMM-Newton* observations from the transition and quiescent phases shows that the increase of the  $N_{\text{H}}$  value by a factor of only 1.16 (Table 3) produces attenuation of the observed fluxes at  $\sim 0.18$  keV by a factor of  $\sim 5$  (see Fig. 2). At the maximum of the 2003 burst, the 0.19 – 0.4 keV emission was not detectable, in spite of the increase of both the luminosity and the temperature of the hot source (Table 3, Fig. 2). The high limiting quantities of  $L_{\text{h}}$  and  $T_{\text{h}}$  are constrained by the minimum flux of photons capable of ionizing hydrogen,  $L_{\text{ph}}(\text{H}) = 8.9 \times 10^{46}$  s<sup>-1</sup>, that is required to give rise the observed high amount of the emission measure,  $EM = 6.2 \times 10^{59} (d/1.1 \text{ kpc})^2 \text{ cm}^{-3}$  (see Eq. (6)). We found that the value of  $N_{\text{H}} \geq 2.5 \times 10^{21} \text{ cm}^{-2}$  is sufficient to damp down the model fluxes ( $\approx 5.5 \times 10^{-10} \text{ erg cm}^{-2} \text{ s}^{-1}$  within the 0.19–0.4 keV range) below a detection level of around  $10^{-16} \text{ erg cm}^{-2} \text{ s}^{-1} \text{ \AA}^{-1}$  for the exposure time used by *XMM-Newton* on 2003/10/10.

According to the model SEDs we ascribe the observed flux anticorrelation to variable wind from the hot star. The wind

particles enrich the plasma surrounding the WD’s photosphere, which increases the number of both the bound-free absorptions (parametrized by  $N_{\text{H}}$  in the model) and the free-bound emissions. The former *attenuates* the supersoft X-ray fluxes, while the latter *increases* the nebular emission.

#### 4.2. Wing profiles and the electron density around the WD

Enhancement of the particle concentration around the hot star is supported independently by our modeling the electron-scattering wing profile of the O VI and He II lines. The model parameter, the optical depth  $\tau_{\text{e}}$  of the electron-scattering layer with the thickness  $r$  is related to its mean electron concentration  $\bar{n}_{\text{e}}$  as

$$\tau_{\text{e}} = \sigma_{\text{T}} \bar{n}_{\text{e}} r. \quad (7)$$

In spite of the model simplification (Sect. 3.2) we approximate the thickness  $r$  of the scattering layer with the radius of the line emitting zone. Having its radius then allow us to estimate the  $\bar{n}_{\text{e}}$  quantity with the aid of Eq. (7). For example, the  $R_{\text{O VI}}$  radius can be obtained from the equation of the equilibrium between the flux of  $L_{\text{ph}}(\text{O V})$  photons, capable of ionizing O V ions, and the number of recombinations by O VI ions. By analogy with Eq. (6), and assuming spherically symmetric nebular medium around the central ionizing source, the equilibrium condition can be expressed as

$$L_{\text{ph}}(\text{O V}) = \frac{4\pi}{3} R_{\text{O VI}}^3 A(\text{O VI}) 0.83 \bar{n}_{\text{e}}^2 \alpha_{\text{B}}(\text{O VI}), \quad (8)$$

where the factor 0.83 is the ratio of protons to electrons,  $A(\text{O VI})$  is the abundance of O VI ions,  $\alpha_{\text{B}}(\text{O VI})$  is the recombination coefficient of a free electron with the O VI ion for the Case B. Substituting the radius of the O VI zone from Eq. (7) to (8), the electron concentration can be expressed as

$$\bar{n}_{\text{e}} = 0.83 \frac{4\pi}{3} \left( \frac{\tau_{\text{e}}}{\sigma_{\text{T}}} \right)^3 A(\text{O VI}) \frac{\alpha_{\text{B}}(\text{O VI})}{L_{\text{ph}}(\text{O V})}. \quad (9)$$

The  $L_{\text{ph}}(\text{O V})$  quantity as a function of the ionizing source temperature is showed in Fig. B.1 of Skopal et al. (2006).

Our model parameters,  $L_{\text{h}}$  and  $T_{\text{h}}$  from quiescent and transition phase (Table 3) correspond to  $L_{\text{ph}}(\text{O V}) = 4.4$  and  $1.7 \times 10^{44} \text{ s}^{-1}$ , respectively. Assuming that all oxygen atoms are ionized to O VI within the zone, i.e.  $A(\text{O VI}) = A(\text{O}) = 4.6 \times 10^{-4}$  (Asplund et al. 2004),  $\alpha_{\text{B}}(\text{O VI}) = 9.5 \times 10^{-12} \text{ cm}^3 \text{ s}^{-1}$  (Gurzadyan 1997) and  $\tau_{\text{e}}$  from Table 2, yield  $\bar{n}_{\text{e}} = 2.6 \times 10^{10} \text{ cm}^{-3}$  ( $R_{\text{O VI}} \doteq 50 R_{\odot}$ ), and  $1.7 \times 10^{11} \text{ cm}^{-3}$  ( $R_{\text{O VI}} \doteq 11 R_{\odot}$ ) during quiescence (2004/06/15–24) and the transition from the burst (2003/11/14–19), respectively.

During the optical maximum of the 2003 hot burst no *FUSE* observation was available. Instead, we modeled the He II  $\lambda 1640$  line from the maximum of the 1995 hot burst (Table 1), because this line is in major part also created at a vicinity of the hot star. In contrast to the quiescent phase, an extended wing profile satisfying the electron-scattering broadening developed at the bottom

of its intense emission core ( $\sim 2.1 \times 10^{-10} \text{ erg cm}^{-2} \text{ s}^{-1} \text{ \AA}^{-1}$ ) at the optical maximum (see Fig. 2, top right). A relatively high optical depth,  $\tau_e = 0.32$  (Table 2),  $L_{\text{ph}}(\text{He II}) = 2.7 \times 10^{46} \text{ s}^{-1}$ ,  $\alpha_{\text{B}}(\text{He II}) = 7.5 \times 10^{-13} \text{ cm}^+ \text{ s}^{-1}$  (Nussbaumer & Vogel 1987) and  $A(\text{He II}) = 0.1$ , yield  $\bar{n}_e = 1.1 \times 10^{12} \text{ cm}^{-3}$  ( $R_{\text{He II}} \approx 6.0 R_{\odot}$ ). The presence of the broad wings of the He II  $\lambda 1640$  line was first pointed out by Viotti et al. (1983) on the *IUE* high-resolution spectra from the 1981 outburst of AG Dra. Simultaneously, they found signatures of the hot star wind suggested by the P Cygni profiles of the N v  $\lambda 1238$ ,  $\lambda 1242$  resonance lines.

#### 4.3. Flux anticorrelation and the nature of bursts

Results of the previous two subsections are mutually complementary. Both the model SEDs and the profile-fitting analysis indicate a significant increase of the particle density around the WD during the bursts of AG Dra. According to other independent analyzes (see e.g. the H $\alpha$  method employed by Skopal 2006), such the increase in the particle density is due to enhanced wind from the hot star into the surrounding particle-bounded nebula. This also explains the nature of this type of the optical bursts, because new emitters will convert the excess of hydrogen ionizing photons in the nebula into the nebular radiation that dominates the optical/near-UV. By return, this mechanism explains the origin of the X-ray–optical/UV flux anticorrelation as the result of variations in the wind from the hot star during different levels of the star’s activity.

Having the result of the reprocessing mechanism, i.e. the parameters of the nebular emission and/or of the wing profiles during bursts and quiescence, we can determine the mass loss rate from the accretor. Generally, the increase of the mass-loss rate via the wind can result from an increase in the mass accretion rate due to an accretion-disk instability. In such the case the enhanced wind provides an important mechanism for removal of angular momentum of rapidly accreted material onto the WD surface (e.g. Duschl 1986; Warner 1995; Livio 1997). From this point of view, the origin of the inverse flux correlation suggests directions for further investigation of the nature of the Z And-type outbursts.

## 5. Summary and conclusions

In this paper we investigated the origin of the supersoft X-ray—optical/UV anticorrelation observed during different levels of activity of the symbiotic binary AG Dra.

We modeled the composite continuum from the supersoft X-rays to near-IR during the maximum of the 2003 burst, the following transition to quiescence and a quiescent phase. We determined physical parameters of individual components of radiation (Fig. 2, Table 3). To support the results obtained by model SEDs we fitted the broad wings of the O vi  $\lambda 1032$ ,  $\lambda 1038$  and the He II  $\lambda 1640$  lines by the Thomson-scattering process. Resulting profile fits and corresponding parameters are shown in Fig. 2 and Table 2, respectively. Main results can be summarized as follows.

1. During the quiescent phase the radiation of the hot stellar source can be reproduced by that of a black body with a radius  $R_{\text{h}} = 0.031(d/1.1\text{kpc})R_{\odot}$  and radiating at the temperature  $T_{\text{h}} = 164\,400 \text{ K}$ , which yields the luminosity  $L_{\text{h}} = 630(d/1.1\text{kpc})^2 L_{\odot}$ . The X-ray emission was attenuated by absorptions corresponding to the neutral hydrogen column density  $N_{\text{H}} = 2.82 \times 10^{20} \text{ cm}^{-2}$  for the ISM abundances that is equivalent to its *interstellar* value (cf. Sect. 1). The

emission measure of the nebular component of radiation was  $EM = 1.3 \times 10^{59}(d/1.1\text{kpc})^2 \text{ cm}^{-3}$ . Fitting parameters for the electron-scattering wings of the O vi doublet (Table 2) and the number of  $L_{\text{ph}}(\text{O V})$  photons from the model SED (Sect. 4.2) correspond to the mean electron concentration around the hot star,  $\bar{n}_e \sim 2.6 \times 10^{10} \text{ cm}^{-3}$ .

2. During the transition phase these parameters changed to  $R_{\text{h}} = 0.036(d/1.1\text{kpc})R_{\odot}$ ,  $T_{\text{h}} = 146\,200 \text{ K}$ ,  $L_{\text{h}} = 530(d/1.1\text{kpc})^2 L_{\odot}$ , and the absorption of the X-ray fluxes corresponded to  $N_{\text{H}} = 3.27 \times 10^{20} \text{ cm}^{-2}$ . The larger quantity of the  $N_{\text{H}}$  parameter reflects an increase in the bound-free absorptions due to an enhanced wind from the hot star. As a result the X-ray fluxes *decreased* relatively to their values from quiescence. In contrast, the nebular emission *increased* to  $EM = 2.2 \times 10^{59}(d/1.1\text{kpc})^2 \text{ cm}^{-3}$ . Simultaneously, flux of the broad O vi wings was by a factor of  $\sim 2$  larger than during quiescence and the model parameters (Tables 2 and 3, Eq. (9)) yield a significantly larger density of  $\bar{n}_e \sim 1.7 \times 10^{11} \text{ cm}^{-3}$  around the hot star, within the O vi zone.
3. During the burst, the high limiting quantities,  $T_{\text{h}} = 180\,000 \text{ K}$  and  $L_{\text{h}} = 1760(d/1.1\text{kpc})^2 L_{\odot}$ , are required to produce the observed large amount of  $EM = 6.2 \times 10^{59}(d/1.1\text{kpc})^2 \text{ cm}^{-3}$ . The negative detection of the supersoft X-ray emission constrains a significant absorption effect that can be parametrized with  $N_{\text{H}} \gtrsim 2.5 \times 10^{21} \text{ cm}^{-2}$ . The strong and extended wings of the He II  $\lambda 1640$  line (Fig. 2) imply a large value of  $\bar{n}_e \sim 1.1 \times 10^{12} \text{ cm}^{-3}$  (Eq. (9)).

Based on these results we formulate the following conclusions:

(i) The model SED demonstrated that the supersoft X-ray emission is produced by the WD photosphere. The X-ray and far-UV fluxes allow us to determine its temperature unambiguously.

(ii) The WD’s continuum spectrum is modified by the circumstellar and interstellar material in the line of sight.

(iii) We found that the source of the opacity, causing the observed anticorrelation between the X-ray and optical/UV fluxes, can be associated with the hot star wind, which enhances during active phases of symbiotic binaries (see Skopal 2006).

(iv) The higher mass loss rate increases the particle density at the vicinity of the WD. This event increases the number of bound-free absorptions in the line of sight, which leads to a significant *attenuation* of the supersoft X-ray photons and, consequently, the free-bound transitions under the Case B *increases* the nebular emission that dominates the optical/near-UV.

(v) The origin of the X-ray–optical/UV flux anticorrelation explains the nature of bursts in AG Dra by reprocessing high-energy photons into the optical through the ionization/recombination events. Understanding the inverse relationship between optical and X-ray fluxes represents an important ingredient in the investigation of the Z And-type outbursts.

*Acknowledgements.* This work is in part based on observations obtained with *XMM-Newton*, an ESA science mission with instruments and contributions directly funded by ESA Member States and NASA. The far ultraviolet data presented in this paper were obtained from the Multimission Archive at the Space Telescope Science Institute (MAST). They were made with the NASA-CNES-CSA Far Ultraviolet Spectroscopic Explorer *FUSE* was operated for NASA by the Johns Hopkins University under NASA contract NASS-32985. The optical spectra were obtained from the archive of the Loiano Station of the Bologna Astronomical Observatory. This research was in part supported by a grant of the Slovak Academy of Sciences No. 2/7010/27. The authors are grateful to the anonymous referee for critical comments and constructive suggestions.

## References

- Anderson, C. M., Cassinelli, J. P., & Sanders, W. T. 1981, *ApJ*, 247, L127

- Asplund, M., Grevesse, N., Sauval, A. J., et al. 2004, *A&A*, 417, 751
- Brown, R. L., & Mathews, W. G. 1970, *ApJ*, 160, 939
- Burstein, D., & Heiles, C. 1982, *AJ*, 87, 1165
- Birriel, J.J., Espey, B.R., & Schutle-Ladbeck, R.E. 2000, *ApJ*, 545, 1020
- Cardelli, J. A., Clayton, G. C., & Mathis, J. S. 1989, *ApJ*, 345, 245
- Castor, J. I., Smith, L. F., & van Blerkom, D. 1970, *ApJ*, 159, 1119
- Corradi, R. L. M., Mikolajewska, J., & Mahoney, T. J. 2003, *Symbiotic Stars Probing Stellar Evolution*, ASP Conf. Ser. 303 (San Francisco: ASP)
- Crudace, R., Paresce, F., Bowyer, S., & Lampton, M. 1974, *ApJ*, 187, 497
- Diplas, A., & Savage, B. D. 1994, *ApJ*, 427, 274
- Duschl, W. J., *A&A*, 163, 56
- Fekel, F. C., Hinkle, K. H., Joyce, R. R., & Skrutskie, M. 2000, *AJ*, 120, 3255
- González-Riestra, R., Viotti, R., Iijima, T., & Greiner, J. 1999, *A&A*, 347, 478
- González-Riestra, R., Viotti, R. F., Iijima, T., Rossi, C., Montagni, F., Bernabei, S., Frasca, A., Skopal, A. 2008, *A&A*, 481, 725
- Greiner, J. Bickert, K., Luthardt, R., Viotti, R., Altamore, A. Gonzalez-Riestra, R., Stencel, R. E. 1997, *A&A*, 322, 576
- Surzadyan, G.A. 1997, *The Physics and Dynamics of Planetary Nebulae* (Berlin: Springer-Verlag), p. 50
- Hummer, D. G., & Mihalas, D. 1967, *ApJ*, 150, L57
- Islaker, H., Nussbaumer, H., & Vogel, M. 1989, *A&A*, 219, 271
- Jansen, F., Lumb, D., Altieri, B., et al. 2001, *A&A*, 365, L1
- Kenyon, S. J., & Webbink, R. F. 1984, *ApJ*, 279, 252
- Kwok, S. 2000, *The Origin and Evolution of Planetary Nebulae* (Cambridge: Cambridge University Press), p. 13
- Livio, M. 1997, in *ASP Conf. Ser. 121, Accretion Phenomena and Related Outflows*, ed. D. T. Wickramasinghe, G. V. Bicknell, & L. Ferrario, (San Francisco: ASP), 845
- Mastrodemos, N., & Morris, M. 1998, *ApJ*, 497, 303
- Mikolajewska, J., Kenyon, S. J., Mikolajewski, M., Garcia, M. R., & Polidan, R. S. 1995, *AJ*, 109, 1289
- Münch, G. 1950, *ApJ*, 112, 266
- Mürset, U., Nussbaumer, H., Schmid, H. M., & Vogel, M. 1991, *A&A*, 248, 458
- Mürset, U., & Schmid, H. M. 1999, *A&AS*, 137, 473
- Nowak, M. A., Wilms, J., & Dove, J. B. 2002, *MNRAS*, 332, 856
- Nussbaumer, H., & Vogel, M. 1987, *A&A*, 182, 51
- Nussbaumer, H., Schmid, H. M., & Vogel, M. 1989, *A&A*, 211, L27
- Osterbrock, D. E. 1989, *Astrophysics of Gaseous Nebulae and Active Galactic Nuclei* (San Francisco: W. H. Freeman and Company Press)
- Schmid, H. M., & Schild, H. 1997, *A&A*, 321, 791
- Schmid, H. M., Krautter, J., Appenzeller, I., et al. 1999, *A&A*, 348, 950
- Seaquist, E. R., Taylor, A. R., & Button, S. 1984, *ApJ*, 284, 202
- Sekeráš, M., & Skopal, A. 2009, (in preparation)
- Skopal, A. 2001, *A&A*, 366, 157
- Skopal, A. 2005, *A&A*, 440, 995
- Skopal, A. 2006, *A&A*, 457, 1003
- Skopal, A. 2007, *New. Astron.*, 12, 597
- Skopal, A., Vittone, A. A., Errico, L., et al. 2006, *A&A*, 453, 279
- Skopal, A., Vaňko, M., Pribulla, T. et al. 2007, *Astron. Nachrichten*, 328, 909
- Sokoloski, J. L., Kenyon, S. J., Espey, B. R., et al. 2006, *ApJ*, 636, 1002
- Wilms, J., Allen, A., & McCray, R. 2000, *ApJ*, 542, 914
- Viotti, R., Ricciardi, O., Ponz, D., Giangrande, A., Friedjung, M., Cassatella, A., Baratta, G. B., & Altamore, A. 1983, *A&A*, 119, 285
- Viotti, R., Altamore, A., Baratta, G. B., Cassatella, A., Friedjung, M. 1984, *ApJ*, 283, 226
- Viotti, R. F., González-Riestra, R., Iijima, T., et al. 2005, *ApSS*, 296, 435
- Warner, B. 1995, *Cataclysmic variable stars* (Cambridge, New York: Cambridge University Press)
- Wegner, W. 2003, *AN*, 324, 219
- Young, P. R., Dupree, A. K., Espey, B. R., Kenyon, S. J., & Ake, T. B. 2005, *ApJ*, 618, 891



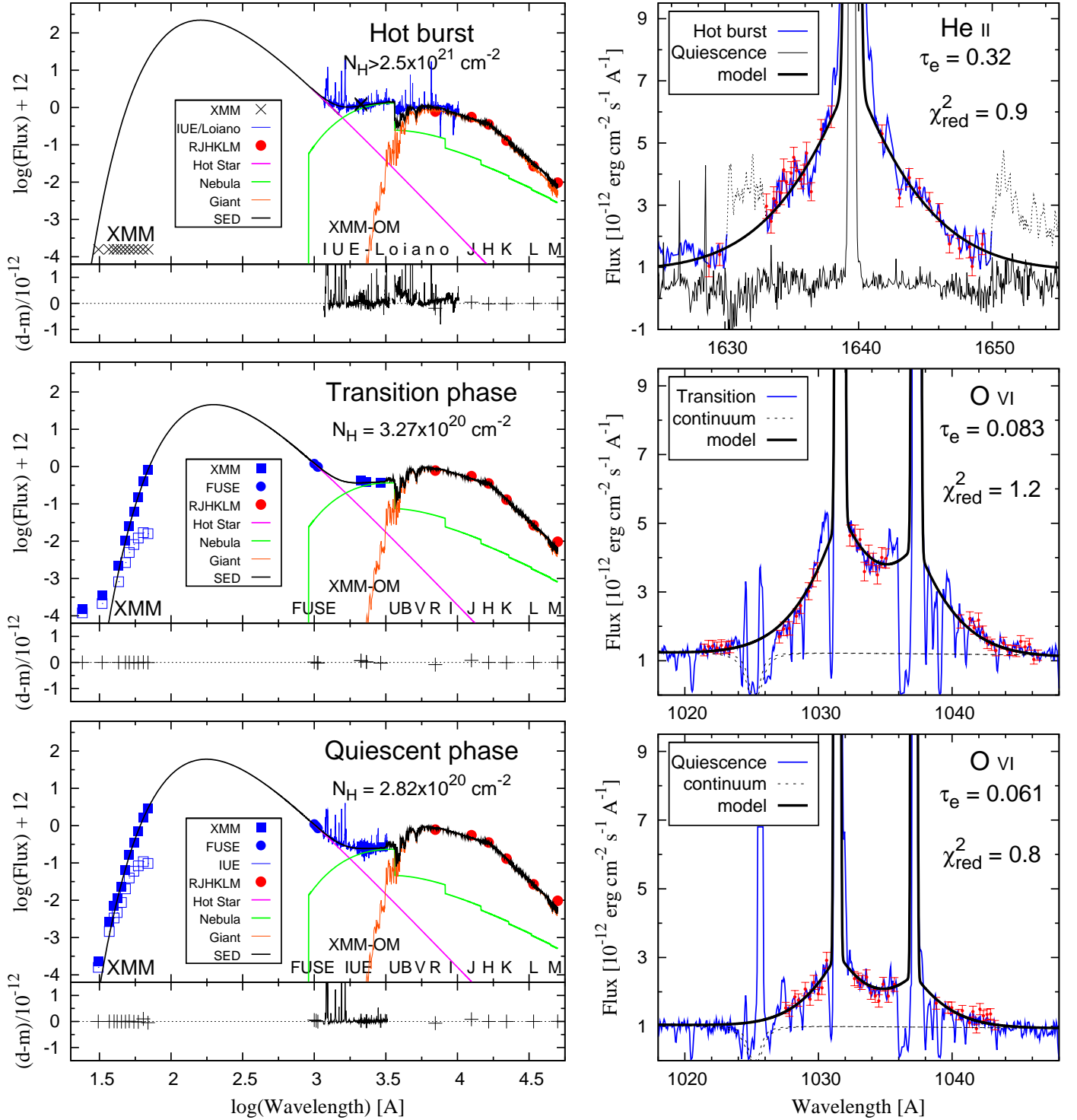


**Fig. 2.** Left panels show a comparison of the observed and modeled SEDs of AG Dra during the hot burst (top), transition phase (middle) and quiescent phase (bottom) with corresponding residuals. Open/filled squares are the observed/corrected X-ray fluxes. They are in units of  $10^{-12} \text{ erg cm}^{-2} \text{ s}^{-1} \text{ \AA}^{-1}$ . Typical uncertainties of the flux-points are around of 10% (Sect. 3.3). Right panels compare the observed and modeled broad wings of the  $\text{O VI}$   $\lambda 1032, \lambda 1038$  doublet and the  $\text{He II}$   $\lambda 1640$  line at these stages of activity. Sample points with uncertainties are plotted in red. Timing of individual observations are given in Table 1. Models are described in Sect. 3 and their parameters are given in Tables 2 and 3.